Chapter 8

Applications of LTE Atmospheres

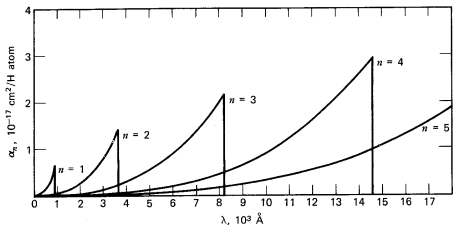

Figure 8.1: The opacity of H^0. The ordinate is the cross-section per neutral hydrogen atom in the given excited state.

Continuum Opacity

Sun

At the point at which $\tau(5000\ \text{Å}) = 2/3$ in the solar atmosphere we have $n_{\rm H} \approx 1.1 \times 10^{17}$, $n_e \approx 4 \times 10^{13}$ cm^{-3} and $T \approx 6200$. We can use the Saha equation to determine the fraction of ionized hydrogen as

$$\frac{n_{\rm H^+}}{n_{\rm H^0}} \approx 2.6 \times 10^{-4}, \tag{8.1}$$

in which we have used $U_{\rm H^0} \approx 2$ and $U_{\rm H^+} = 1$. The hydrogen in the solar atmosphere is overwhelmingly neutral.

The continuum opacity of neutral hydrogen depends on the degree of excitation. For example, the Lyman continuum at $\lambda < 912$ Å corresponds to ionizations from the $n = 1$ level, the Balmer continuum for $\lambda < 3647$ Å corresponds to ionizations from the $n = 2$ level, and the Paschen continuum for $\lambda < 8206$ Å corresponds to ionizations from the $n = 3$ level. In the optical, we are concerned with the Paschen continuum, and so we need to calculate the excitation of the $n = 3$ level

$$\frac{n_{{\rm H}^0_{n=3}}}{n_{\rm H^0}} \approx 1.4 \times 10^{-9}. \tag{8.2}$$

Thus, although almost all of the hydrogen in the Solar atmosphere is neutral, almost none of it is in a state in which it can contribute to the opacity in the visual.

We can also calculate the relative abundance of H^-. This is a stable bound state consisting of a proton and two electrons and has an ionization potential of 0.754 eV. It has no bound excited states above the ground state and so we have $U_{\rm H^-} = 1$, because the electrons in the ground state must have opposite spins. We find

$$\frac{n_{\rm H^-}}{n_{\rm H^0}} \approx 3.5 \times 10^{-8}. \tag{8.3}$$

Thus, H^- is very rare in the solar atmosphere, but is roughly 25 times more common than neutral hydrogen in the $n = 3$ state. Since the continuum cross-sections for bound-free transitions are roughly similar (2.4×10^{-17} cm^2 for neutral hydrogen at the Paschen edge and about 4×10^{-17} cm^2 for H^- at its peak at roughly 8500 Å), bound-free absorption by H^- dominates the optical continuum opacity.

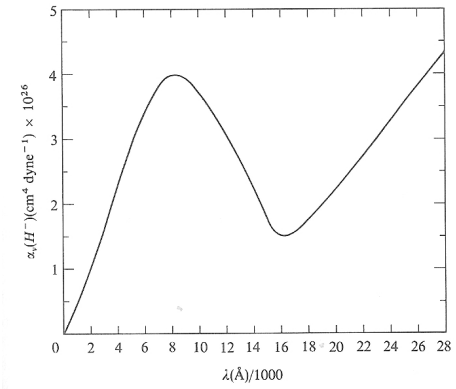

Figure 8.2: The opacity of H^- at 6300 K. The ordinate is the cross-section per neutral hydrogen atom and per unit electron pressure $n_e kT$. The opacity below 1.6 μm is dominated by bound-bound absorption and above 1.6 μm by bound-free absorption.

Since the absorption coefficient is the product of the cross-section per absorber and the density of absorbers, we might expect that it should be linear in the total density. However, consideration of H^- absorption in cool stars shows that this is not always the

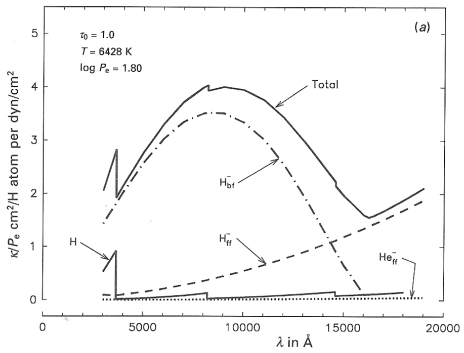

Figure 8.3: The opacity in the optical under conditions typical of the solar photosphere. The opacity is dominated by H^-.

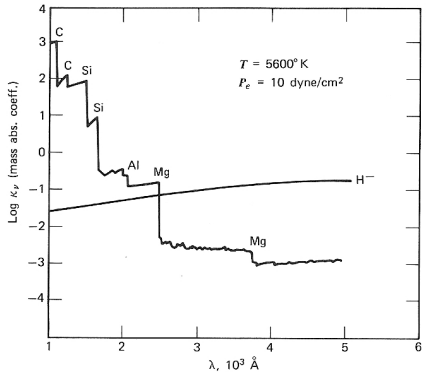

Figure 8.4: The opacity in the UV and optical under conditions typical of the solar photosphere. The UV opacity is dominated by bound-free absorption of Mg, Al, Si, and C.

case. We can write the Saha equation for H^- as

$$\alpha = a_{H^-} n_{H^-} \tag{8.4}$$

$$= a_{H^-} \frac{n_{H^0} n_e}{n_S} e^{\chi/kT} \tag{8.5}$$

$$\propto n n_e. \tag{8.6}$$

In the Sun, $n_p \approx 2.9 \times 10^{13}$ cm^{-3} $\approx 0.75 n_e$. Thus, in the Sun and hotter stars the dominant source of electrons is hydrogen. The Saha equation for ionization of hydrogen then gives $n_e n_p \propto n$ and since $n_e \approx n_p$ this leads to $n_e \propto n^{1/2}$. The absorption coefficient then becomes

$$\alpha \propto n^{3/2}. \tag{8.7}$$

This is more complicated than the simple $\alpha \propto n$ that we would expect of the relative fraction of absorbers was constant. This behaviour leads to important differences between the atmospheres of cool giants (low density) and dwarfs (higher density). We'll see a slightly different dependence of the H^- opacity on density in cooler stars below.

Above 1.65 μm, H^- continues to dominate, but now by free-free absorption. In the ultraviolet above 912 Å, ionization of Mg, Al, Si, and C and Rayleigh scattering dominate the continuum opacity. Line blanketing is important in the blue and the ultraviolet. Below 912 Å absorption by neutral hydrogen from the $n = 1$ ground state dominates.

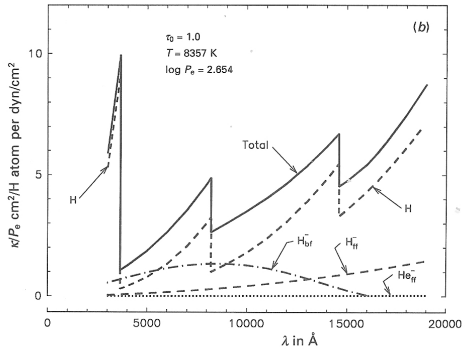

Figure 8.5: The opacity in the optical under conditions typical of a late A dwarf. The opacity is dominated by H^- immediately above the Balmer jump and H^0 immediately below the Balmer jump.

Hotter Stars

A stars are hotter then the Sun, so the same point at which $\tau(5000 \text{ Å}) = 2/3$ in the atmosphere of an A dwarf with $T_{\rm eff} \approx 8000$ K would have $n_H \approx 1.8 \times 10^{16}$, $n_e \approx 7.5 \times 10^{14}$ cm^{-3} and $T \approx 8800$ K. Under these conditions, hydrogen is still largely neutral with

$$\frac{n_{H^+}}{n_{H^0}} \approx 4.4 \times 10^{-2}. \tag{8.8}$$

However, the degree of ionization is now quite significant – almost 5% compared to less than 0.03% in the Sun – and so hydrogen supplies almost all of the electrons and we have $n_{H^+} \approx n_e$.

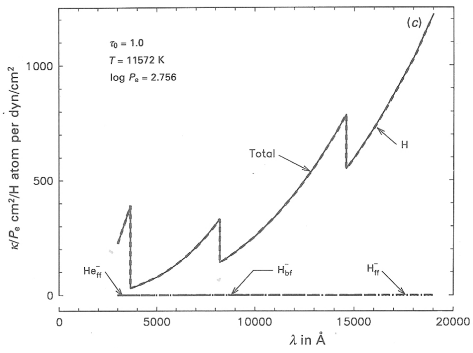

Figure 8.6: The opacity in the optical under conditions typical of a late B dwarf. The opacity is dominated by H^0 both immediately above and immediately below the Balmer jump.

The abundance of H^- is also higher than in the Sun with

$$\frac{n_{H^-}}{n_{H^0}} \approx 2.5 \times 10^{-7}. \tag{8.9}$$

However, the abundance of neutral hydrogen in the $n = 3$ level is also higher, with

$$\frac{n_{H^0_{n=3}}}{n_{H^0}} \approx 1.1 \times 10^{-6}. \tag{8.10}$$

In these stars, absorption by the Paschen continuum is more important than bound-free absorption by H^-. This trend increases through the A stars, but eventually hydrogen becomes sufficiently ionized that first He0 becomes important in the B stars and finally He+ becomes important in the O stars. Electron scattering is also important in O stars.

At points at which the bound-free opacity is small, such as just redward of the Balmer jump in early A and late B stars, electron scattering opacity can be important. In the ultraviolet, metals such as C, N, O, Ne, and Si continue to be important.

Cooler Stars

H^- continues to be an important source of opacity in stars cooler than the Sun. In these stars, the ionization fraction of hydrogen is very low, and the principal source of electrons is ionization of metals, and so $n_e \propto x_M n$, where x_M is the fractional metal abundance. We then have

$$\alpha \propto x_M n^2. \tag{8.11}$$

Again, this is more complicated than the simple $\alpha \propto n$ that we would expect of the relative fraction of absorbers was constant. This behaviour leads to important differences between the atmospheres of cool metal-poor and metal-rich stars.

In stars cooler than mid-M, molecular hydrogen and its ions can exist. H_2 itself does not absorb in the optical, but H_2^+ and H_2^- can be important. Much more important, though, is line blanketing by first metallic lines and then by molecules.

Balmer Jump

The Balmer jump at 3647 Å is an interesting diagnostic of conditions in the stellar atmosphere. It depends largely on the ratio of the opacities on either side of 3647 Å. If the opacities are similar, the continuum on both sides of the jump will be formed at similar places in the atmosphere and so will be smooth and not display a large jump. If the opacity on the blue side is larger, the continuum here will be formed higher in the atmosphere at cooler temperatures than the continuum on the red side, and we would expect a large jump.

In F and G stars ($T_{\rm eff} \approx 5000$–7500 K), the opacity longward of the jump is largely due to H^- whereas the opacity shortward of

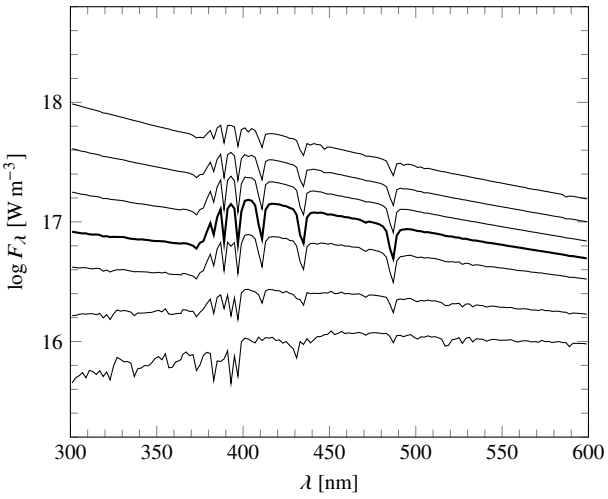

Figure 8.7: Emergent fluxes for ATLAS9 model atmospheres for $\log g = 5.0$ and $T_{\rm eff} = 6000$, 7000, 8500, 10000 (thick), 12000, 15000, and 20000 K. Note that slope of the Paschen continuum (above 370 nm) becomes bluer with increasing temperature whereas the strength of the Balmer jump at 365 nm first increases and then decreases with effective temperature.

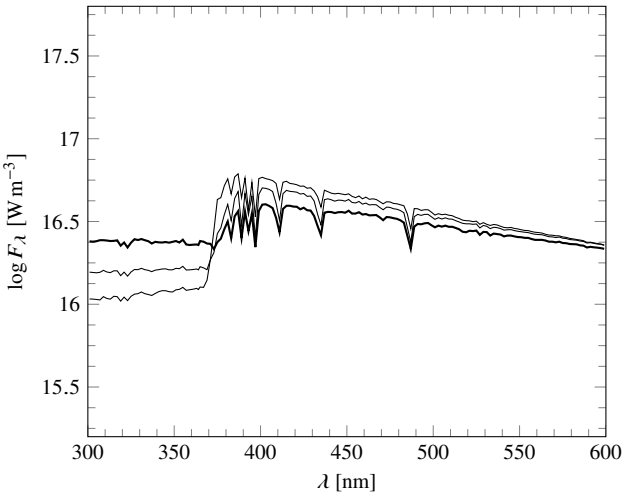

Figure 8.8: Emergent fluxes for ATLAS9 model atmospheres for $\log g = 1.0$, 3.0, and 5.0 (thick) and $T_{\rm eff} = 7500$ K. Note that for stars of this temperature, the strength of the Balmer jump at 365 nm increases as the surface gravity decreases.

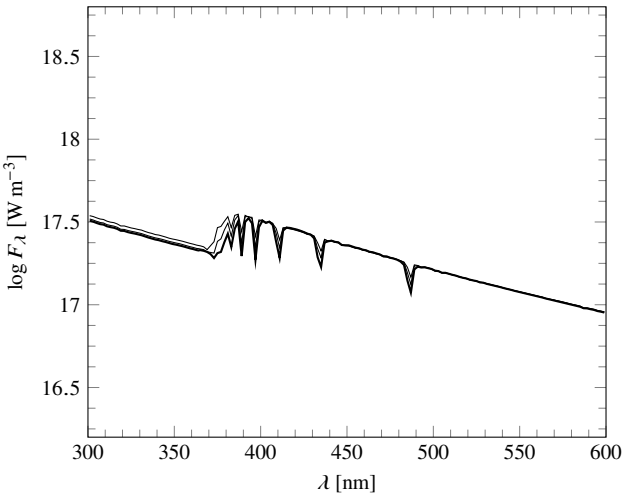

Figure 8.9: Emergent fluxes for ATLAS9 model atmospheres for $\log g = 3.0$, 4.0, and 5.0 (thick) and $T_{\rm eff} = 14000$ K. Note that for stars of this temperature, the strength of the Balmer jump at 365 nm does not depend strongly on the surface gravity.

the jump is due to both H^- and bound-free absorption from the $n = 2$ level of H^0. The ratio of opacities is then

$$\frac{\alpha(3647^- \text{ Å})}{\alpha(3647^+ \text{ Å})} \approx \frac{a_{\rm H^-} n_{\rm H^-} + a_{{\rm H}^0_{n=2}} n_{{\rm H}^0_{n=2}}}{a_{\rm H^-} n_{\rm H^-}} \tag{8.12}$$

$$= 1 + \frac{a_{{\rm H}^0_{n=2}}}{a_{\rm H^-}} \frac{n_{{\rm H}^0_{n=2}}}{n_{\rm H^-}} \tag{8.13}$$

If we use the Saha and Boltzmann equations to determine the relative densities of H^- and H^0 in the $n = 2$ state, we can write

$$\frac{\alpha(3647^- \text{ Å})}{\alpha(3647^+ \text{ Å})} \approx 1 + \left(\frac{a_{{\rm H}^0_{n=2}}}{a_{\rm H^-}}\right)\left(\frac{8 n_{\rm S}(T) e^{-(\chi_{\rm H^-} + E_{n=2})/kT}}{n_e}\right). \tag{8.14}$$

We can see then that the Balmer jump depends on both the temperature and the electron density and can be used to determine one given the other. The jump becomes stronger with increasing temperature (recall that $n_{\rm S} \propto T^{3/2}$) and with lower density. We would expect it to strengthen towards earlier spectral classes and towards decreasing surface gravity. This is exactly what is observed in Figures 8.7, 8.8, and 8.10 for effective temperatures of 5000–7500 K appropriate for FG stars.

For dwarf stars hotter than about 9000 K, the excitation of the $n = 3$ level is sufficiently large that that Paschen continuum overtakes H^- bound-free absorption as the principal source of opacity longward of the Balmer jump. In these stars,

$$\frac{\alpha(3647^- \text{ Å})}{\alpha(3647^+ \text{ Å})} \approx \frac{a_{{\rm H}^0_{n=3}} n_{{\rm H}^0_{n=3}} + a_{{\rm H}^0_{n=2}} n_{{\rm H}^0_{n=2}}}{a_{{\rm H}^0_{n=3}} n_{{\rm H}^0_{n=3}}} \tag{8.15}$$

$$\approx 1 + \left(\frac{a_{{\rm H}^0_{n=2}}}{a_{{\rm H}^0_{n=3}}}\right)\left(\frac{4}{9} e^{1.89 {\rm eV}/kT}\right), \tag{8.16}$$

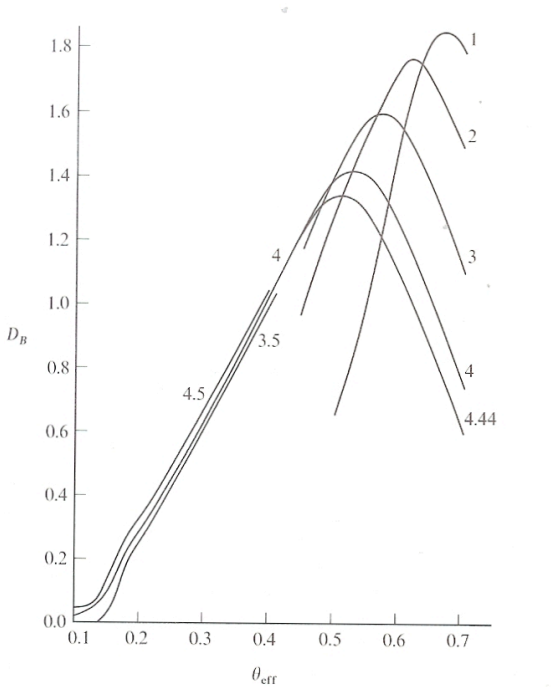

Figure 8.10: The Balmer jump $D_B \equiv 2.5 \log[F_\lambda(3647+)/F_\lambda(3647-)]$ calculated from LTE model atmospheres as a function of inverse effective temperature $\theta_{\rm eff} \equiv (5040 \text{ K})/T_{\rm eff}$. The curves are labelled with $\log g$. Note that the Balmer jump depends on temperature and gravity for stars cooler than about 10,000 K but only on temperature for hotter stars.

Table 8.1: Strömgren Filters

Filter	Name	$\bar{\lambda}$ (nm)	$\Delta\lambda$ (nm)
u	ultraviolet	350	30
v	violet	411	19
b	blue	467	18
y	yellow	547	23

where the factor of 4/9 comes from the relative degeneracies (8 and 18) of the $n = 2$ and $n = 3$ levels and 1.89 eV is the energy difference between the $n = 2$ and $n = 3$ levels. Here the Balmer jump depends on temperature and not density, and furthermore is a decreasing function of temperature. This is seen in Figures 8.7, 8.9, and 8.10 for effective temperatures of 9000–25,000 K appropriate for BA stars.

At higher temperatures and at the low densities encountered in supergiants, electron scattering becomes important, first on the red side of the jump and then even on the blue side. In these stars, the Balmer jump again becomes a function of both density and temperature.

Strömgren Photometry

Strömgren defined a four-color $uvby$ photometric system based on intermediate width filters ($\Delta\lambda$ of 18–30 nm compared to 160–210 nm for the Johnson UBV filters). As we can see in Figure 8.11, the u filter lies in the Balmer continuum below the Balmer jump and the vby filters lie in the Paschen continuum above the Balmer jump. The y magnitude of a star is closely correlated to the V magnitude. The Strömgren filters were designed specifically to determine the parameters of stars. Their advantage compared to the Johnson filters is that they are much better attuned the the spectral features of stars; for example, the Strömgren u filter is completely below the Balmer jump, whereas the Johnson U filter straddles the Balmer jump.

Photometry with Strömgren filters is normally presented in terms of the y magnitude, the $b - y$ color, and the c_1 and m_1 indices, which are defined by

$$c_1 \equiv (u - v) - (v - b) \tag{8.17}$$

and

$$m_1 \equiv (v - b) - (b - y). \tag{8.18}$$

Note that c_1 and m_1 are differences between adjacent colors. Since colors measure in some sense the slope (first derivative) of a spectrum, the difference between two colors measures the curvature (second derivative) of a spectrum.

The $b - y$ color measures slope in Paschen continuum, which as we have see is well-correlated with the effective temperature for BAFG stars (e.g., in Figure 8.7). Thus, $b - y$ is an effective temperature indicator in these stars.

Table 8.2: Strömgren Diagnostics in BAFG Stars

Measurement	BA	FG
$b - y$	$T_{\rm eff}$	$T_{\rm eff}$
$c_1 = (u - v) - (v - b)$	$T_{\rm eff}$	$\log g$
$m_1 = (v - b) - (b - y)$		Z

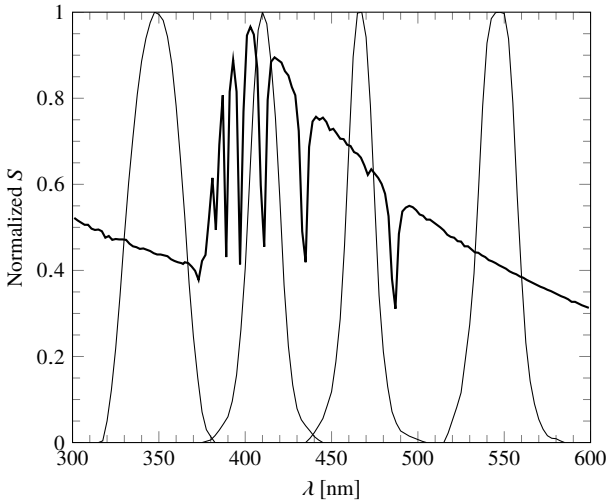

Figure 8.11: The Strömgren $uvby$ filters compared to the flux from a model atmosphere with $T_{\rm eff} = 10,000$ K and $\log g = 5.0$. Notice that the u filter is below the Balmer jump at 346 nm wherease the vby filters are above it, which allows $c_1 \equiv (u - v) - (v - b)$ to be used as a indicator of the strength of the Balmer jump.

The c_1 index measures the curvature in the uvb region; the Balmer jump falls between u and v, so c_1 will measure the strength of the Balmer jump (see also Figure 8.11). Thus, c_1 is a surface gravity indicator for FG stars and an effective temperature indicator in BA stars.

Figure 8.12 shows a calibration of $b - y$ and c_1 for effective temperature and gravity. It shows that for temperatures from 5500 to 8000 K, we can determine both the effective temperature and the surface gravity. Above 8000 K, we lose the ability to discriminate surface gravity from c_1. (We will shortly see how we can extend the Strömgren system to remedy this deficiency.)

The m_1 index measures the curvature in the vby region. This region lies in the Paschen continuum, so at first it might appear that there should be little variation in the curvature. However, in F and G stars, v lies in a region that has several iron lines as well as the CN bands at 4142 Å and 4215 Å, whereas b and y lie in regions that are largely free of lines (see also Figure 8.13). Thus, differences in curvature in this region can be caused by variations in metallicity, as increasing metallicity reduced the flux in the v filter more than in the b and y filters. Thus, m_1 is a metallicity indicator in F and G stars.

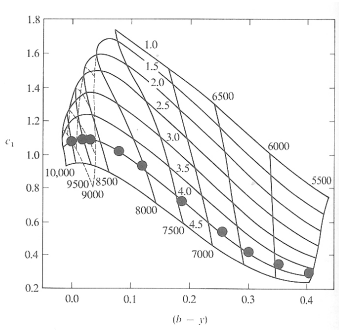

Figure 8.12: The c_1 index as a function of $b - y$. The grid shows the projection of a grid of LTE model atmospheres with different effective temperatures and gravities. The dots show the observed values of stars on the main sequence (which have $\log g \approx 4$). For stars between 8000 K (A5) and 5500 K (G7), the colors depend unambiguously on the effective temperature and gravity. Above 8000 K, the relation between colors and effective temperature and surface gravity is double valued.

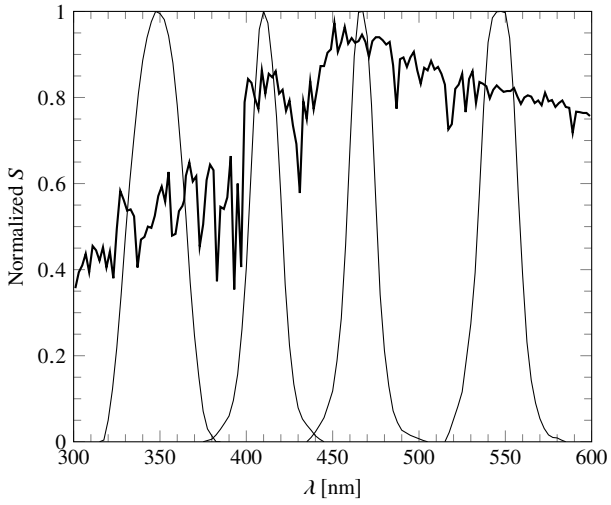

Figure 8.13: The Strömgren $uvby$ filters compared to the flux from a model atmosphere with $T_{\rm eff} = 6000$ K and $\log g = 5.0$. Notice the strong metal absorption lines in the v filter around 410 nm, which allows $m_1 \equiv (v - b) - (b - v)$ to be used as a metallicity indicator for FG stars.